Supplement of Atmos. Chem. Phys., 20, 15635–15664, 2020
https://doi.org/10.5194/acp-20-15635-2020-supplement

Supplement of

Measurements to determine the mixing state of black carbon emitted from the 2017–2018 California wildfires and urban Los Angeles

Joseph Ko et al.

Correspondence to: George Ban-Weiss (banweiss@usc.edu)

S1 Source-to-receptor timescale estimations

This section describes the methods used to arrive at the approximate source-to-receptor timescales shown in Table 2. For L1, a semi-quantitative range was estimated by examining CAMS model output and MODIS imagery/data. The CAMS model and MODIS data both show that long-range transport from East Asia and Oregon wildfires during the first campaign (September 2017) took at a minimum several days to arrive at the sampling site from the approximate location of the respective sources. The upper end of the range for L1 is determined by the approximate maximum lifetime of BC as mentioned in previous literature (Bond et al., 2006; Lund et al., 2018). The upper end for L3, L8, L9, and L10 were also approximated by the same logic.

The timescale for L2 was also determined semi-quantitatively. Since it was determined that local sources were heavily impacting the measurements during this period, we estimated that a timescale on the order of minutes to hours was appropriate, given that the closest source of substantial emissions would be right off the dock at the USC Wrigley Institute, which was ~100 m away from the inlet.

The lower end for L3 was determined by observing CAMS model output and determining how long it took for the $PM_{2.5}$ emissions plume from the Thomas Fire (and urban emissions) to recirculate back to Catalina Island. See video 2 of the Video Supplement for visual support.

The approximations for L4 to L7 were determined using the following steps. First, four HYSPLIT back-trajectories were chosen for examination: (1) a back-trajectory starting an hour prior to the beginning of the LEO period, (2) a back-trajectory starting at the beginning of the LEO period, (3) a back-trajectory starting at the end of the LEO period, and finally (4) a back-trajectory starting an hour after the end of the LEO period. For each of these four back-trajectories, the first hour at which the trajectory crossed over the California coast was determined. From this, we approximated how many hours it took for a particle to travel between the inlet and the coastal edge of the Los Angeles basin. The mean "inlet-to-coast" timescale was then calculated for the four back-trajectories. The floor of this value is what is shown in Table 3 as the approximate characteristic timescale for the time periods, L4 to L7. The floor of the mean was used because this would conservatively round to the nearest integer value of the timescale by representing the *shortest* length of time it would take for a particle to travel from an emission source on land to the sampling site on Catalina Island.

For L8 to L10, CAMS model and MODIS imagery/data were used to establish an upper and lower limit of approximate timescales. For example, video 3 and 4 in the Video Supplement show that the plume of aerosols from the Camp Fire takes at least a few days to reach the Southern California region. This established the lower end limit of ~days. As mentioned previously, the upper end of ~weeks is from established knowledge about the approximate lifetime of aerosols in the atmosphere.

S2 Details regarding section 3.1: source identification and meteorology

The red trajectories in Fig. 3 represent seven-day back-trajectories starting at 00:00 Pacific Daylight Time for every day of the first campaign (September 2017). These back-trajectories show that the dominant wind-flows during the first campaign were westerly, which is consistent with the typical synoptic winds that blow toward the Los Angeles coast from the Pacific Ocean, as well as the westerly mesoscale flows driven by the sea breeze. Wind data from Los Angeles International Airport, Long Beach Airport, and Avalon (Fig. 2) further confirm that winds were generally blowing from the west during the first campaign. The back-trajectories and wind data suggest that measured particles during the first campaign are "aged" since there are limited major nearby sources that are upwind of the sampling site. Although the exact sources of BC during this period cannot be ascertained, the plausible sources of rBC-containing particles would be from (1) nearby ships and aviation, (2) aged urban and/or biomass burning emissions, and/or (3) inter-continental transport from East Asia. Using CAMS model data, we further identified two long-range sources that likely contributed to measured rBC-containing particles; these model data identified large biomass burning events during the first campaign in Oregon and Northern California. Although these fires were much further away than the Southern California fires that were active during the second and third campaigns (December 2017, November 2018), close visual tracking of plumes from these fires with the CAMS visualization tool and NASA aerosol index product shows that $PM_{2.5}$ from these fires reached the coast of California, even as far south as Catalina Island (i.e., our sampling site) (see Fig. S4). We also identified an example of inter-continental transport of $PM_{2.5}$ from East Asia around the time of the first campaign using CAMS data (see Fig. S6). We did not attempt to determine which potential sources were dominant for the first campaign, but regardless of the source it is fair to say that measured rBC-containing particles were aged.

In strong contrast to the first campaign (September 2017), the second and third campaigns (December 2017, November 2018) included periods in which the sampling location was downwind of biomass burning and urban emissions. The yellow and green trajectories in Fig. 3b and 3c represent 72-hour back-trajectories for each hour of the second and third campaigns. These back-trajectories, along with supporting airport wind data (Fig. 2), confirm that winds were easterly-to-northerly for a significant fraction of these campaigns. These "Santa Ana" conditions, in which winds originate from dry desert regions north and east of Los Angeles and advect through the mountain ranges of Southern California to the Los Angeles basin (Small, 1995), are infamous for exacerbating wildfires. Figs. 3d and 3e show several HYSPLIT trajectories either going through or coming within close proximity to active wildfires in the Southern California region (see Table 1 for information on wildfires). This provides evidence that the measured rBC-containing particles in the second and third campaign included important contributions from both fresh biomass burning emissions, and fresh urban emissions from the Los Angeles basin, which are largely from motor vehicles.

Since meteorology varied a lot more during the second and third campaigns compared to the first campaign, different periods of interest within these campaigns were examined more carefully in an attempt to assess the relative impact of different known sources. For the second campaign (December 2017), we examined the time periods defined by unique peaks in rBC loading (discussed in section 3.2 and labeled in Fig. 5). After investigating HYSPLIT back-trajectories, CAMS model data, and airport wind data, we concluded that contributions from the Thomas Fire (Table 1) and urban emissions from the Los Angeles basin were too difficult to accurately distinguish from one another. The Thomas Fire and Los Angeles urban plumes were within ~110 km (~70 miles) of each other, and even though the CAMS model output (Fig. S5) shows two distinct plumes around the time of Peak P1 from the second campaign (Fig. 5 and discussed in Section 3.2), both plumes likely interacted and impacted measurements throughout the second campaign. Thus, we conclude that both the Thomas Fire and Los Angeles urban emissions were the main sources of measured rBC during the second campaign, when Santa Ana wind conditions were blowing emissions towards the sampling site.

Although the relatively low fraction of thickly-coated rBC particles and low average coating thickness (discussed in section 3.3 and 3.5) might seem to suggest that local biomass burning emissions were not impacting the second and third campaigns, various data show otherwise. First, Soleimanian et al. (2020) reported elevated concentrations of levoglucosan (a biomass burning tracer) during the second and third weeks of November, which overlaps with the third campaign (12-18 November 2018). The weekly mean concentration of levoglucosan was reported to be 187.5 ng m^{-3} for the week of 7 to 14 November 2018, and 83.89 ng m^3 for the week of 15 to 22 November 2018. For reference, levoglucosan concentrations during July 2018 (non-wildfire season) ranged between ~4 and 17 ng m^{-3}. This removes any lingering doubt whether or not biomass burning emissions contributed to the broader LA basin plume during this period. There were no levoglucosan measurements available for the second campaign (December 2017), but given a similar geographic situation (large wildfire close to the LA basin) and similar Santa Ana wind conditions, it would be hard to imagine a fire like the Thomas Fire not affecting measurements on Catalina Island during the second campaign as well.

To provide an additional line of evidence to fill in for the missing levoglucosan measurements during the second campaign (December 2017), the HYSPLIT dispersion model was run for both 21 and 22 December 2017, simulating a controlled burn with an identical area as the burn area of the Thomas Fire and the Creek Fire. The results are shown in Fig. S20 and S21, and they show beyond reasonable doubt that the plume fingerprint reaches the sampling location on Catalina Island during the second campaign. CALIPSO lidar images for the second and third (November 2018) campaigns were also qualitatively analyzed and reported here in Fig. S9 to S19. According to the CALIPSO aerosol classification algorithm, there were many instances during the second and third campaign in which biomass burning aerosols were present off the coast of Southern California. This supplemental data further bolsters our initial hypothesis that local Southern California wildfires were contributing to the broader LA plume. Nonetheless, we cannot quantitatively apportion the relative effect of the urban emissions versus local biomass burning emissions during these time periods. Based on the mixing state measurements and rBC core size distributions, we conservatively conclude that although biomass burning emissions were affecting measurements during this time of relatively low coating thickness, urban emissions seem to be the dominant source type. Although we cannot eliminate the possibility of relatively thinly-coated biomass burning rBC particles during the second and third campaigns, there is also no way for us to definitively prove or disprove this with the available data.

For the third campaign (November 2018), the CAMS model and MODIS satellite imagery show a large plume of aerosols from Northern and Central California fires (particularly the Camp Fire, Table 1) reaching Southern California (see video 3 of Video Supplement). Figure S7 confirms that back-trajectories from this period originate from the area of the plume that is visible in the eight-day mean AOD overlay (9 to 16 November 2018). The AOD overlay represents the general extent of the Camp Fire plume ~1-4 days before the start of the period with increased concentrations. The back-trajectories overlaid on the AOD layer suggest that the measured rBC-containing aerosols during the last two days of the third campaign did indeed originate from within the Camp Fire plume. This particular period can be further examined in the supplemental video of animated $PM_{2.5}$ concentration isopleths output by the CAMS model for the third campaign (see video 1 of Video Supplement). In the first part of the third campaign prior to Camp Fire contributions, measured rBC likely included contributions from a mixture of fresh biomass burning and urban emissions because the Woolsey fire was located within ~45 km (~30 miles) of the broader Los Angeles urban plume. We could not isolate contributions from the Woolsey Fire (Ventura) and Los Angeles urban emissions during this period.

S3 Details regarding section 3.4: negative lag-times and rBC morphology

According to Sedlacek et al. (2015) higher laser power and higher sample flow rates result in more rapid rBC heating, and therefore higher rates of fragmentation (i.e., larger $f_{lag,neg}$). In this study, a laser current of 1600 mA was used for the first and second campaign, and a laser current of 1850 mA was used for the third campaign. The sample flow rate was set to 120 cm^3 min^{-1}. Comparatively, Sedlacek et al. (2012) reported a laser current of 3000 mA and sample flow rate of 120 cm^3 min^{-1}. Given that Sedlacek et al. (2015) found a six-fold increase in $f_{lag,neg}$ by increasing the laser current from 2000 mA to 3000 mA (with the same sample flow rate), it was expected that $f_{lag,neg}$ in this study would be much lower than $f_{lag,neg}$ reported by Sedlacek et al. (2012). Taking the operating conditions into account and multiplying the $f_{lag,neg}$ in this study by an adjustment factor of ~7 (1850 mA versus 3000 mA, see Fig. 8 in Sedlacek et al., 2015), the November 2018 peaks observed in the $f_{lag,neg}$ time series in Fig. 6 would increase from ~0.06 to ~0.41, which is much closer to the 0.6 value reported by Sedlacek et al. (2012).

S4 Supplemental figures

Figure S1. Photo showing the sample inlet, which was positioned on the roof of USC's Wrigley Institute on Catalina Island. Map data © Google Earth.

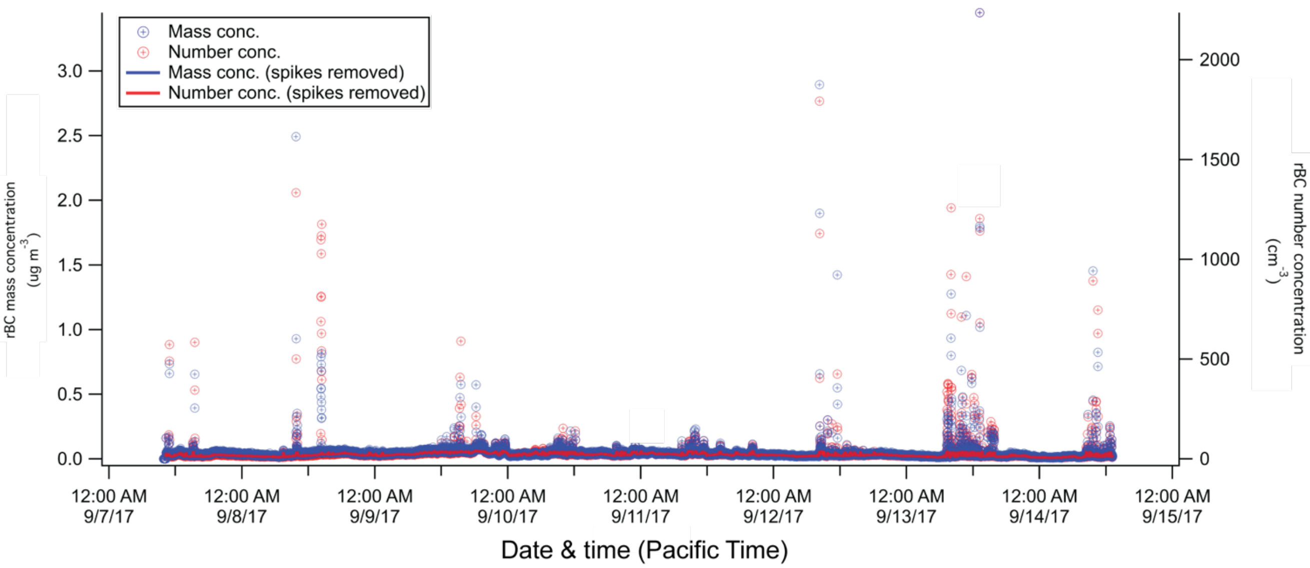

Figure S2. rBC mass and number concentration for the September campaign. The circle markers indicate all points, including the spikes. The solid lines represent the concentration time series after filtering out the spikes.

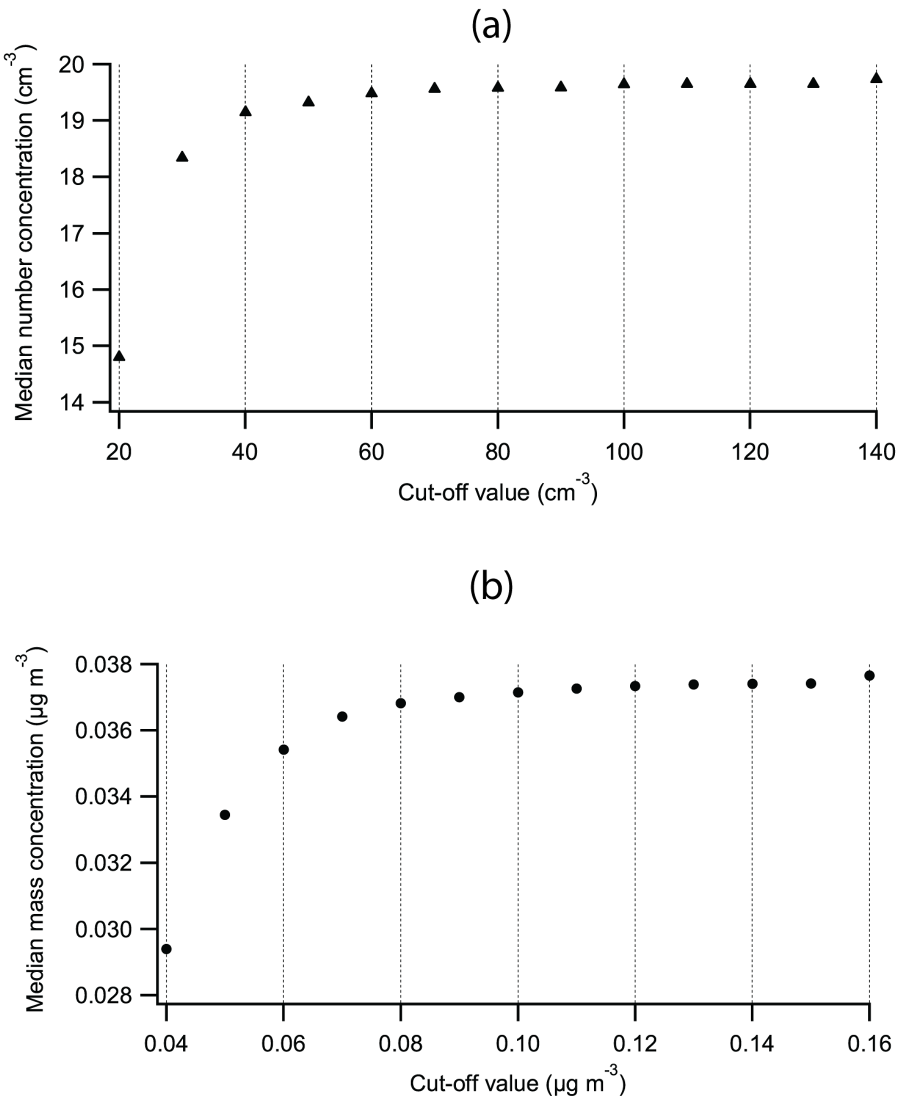

Figure S3. Median number concentrations (a) and mass concentration (b) for the September campaign, shown as a function of the spike threshold cut-off values (see Section 2.5). The median concentrations display an asymptotic behaviour.

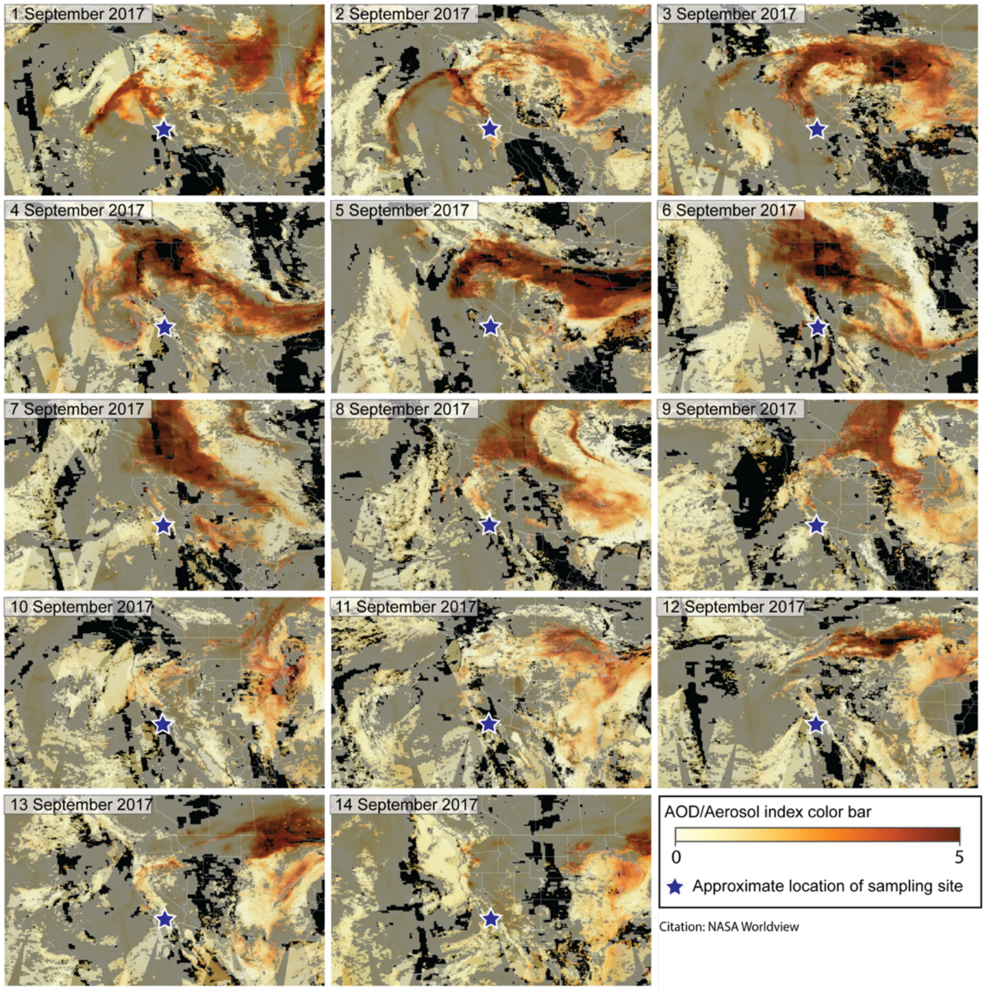

Figure S4. Aerosol optical depth (AOD) and aerosol index layers (NASA MODIS) imposed on top of each other, from 1 to 14 September 2017 (during the first campaign). Darker red indicates higher concentrations of aerosols. The large aerosol plume is largely from the Oregon fires that were active during this period. The blue star indicates the approximate location of the sampling site, and the progression of images show that the plume from the Oregon fires likely contributed to measured rBC during the first campaign (September 2017). Aerosol index was layered below the AOD layer in order to visually "fill" some gaps in the qualitative representation of the aerosol plume. Gaps in the AOD and aerosol index layer are due to cloud cover, and spatial variation in the gaps are due to NASA satellite routes.

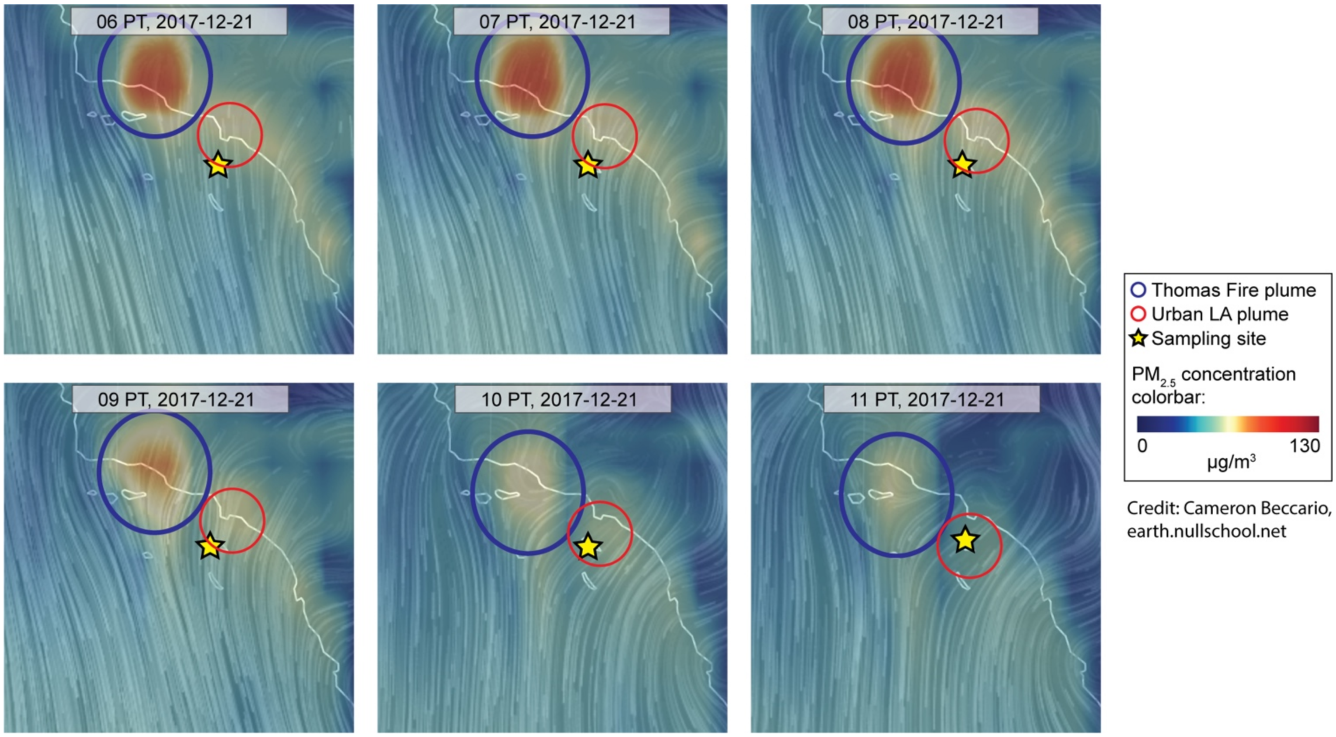

Figure S5. CAMS $PM_{2.5}$ model visualizations from 06 to 11 Pacific Time, on 21 December 2017, ordered chronologically for every hour, starting from the top-left and ending at the bottom-right sub-figure. This time period corresponds to Peak P1 of the December campaign (see Figure 5 in the main body). The blue circle shows the distinct plume from the Thomas Fire in Santa Barbara/Ventura County. The red circle shows a less pronounced, but distinct, plume from emissions in the Los Angeles urban basin, presumably mostly from motor vehicle emissions. The green circle denotes the sampling location on Catalina Island. Concentration colorbar gradient ranges from red to blue, where red represents high concentrations and vice versa.

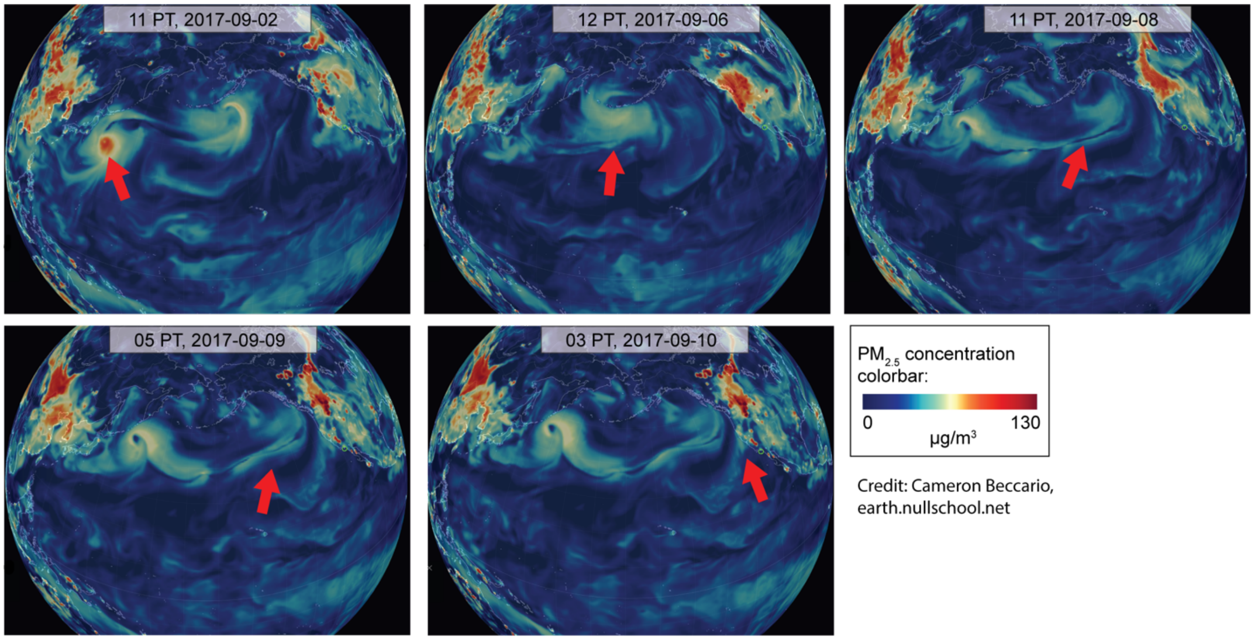

Figure S6. CAMS $PM_{2.5}$ model visualizations showing a plume originating from the East Asia region and advecting across the Pacific Ocean towards California during the time of the first campaign (September 2017). The first sub-figure is a snapshot at 11 Pacific Time on 2 September 2017. The last sub-figure is a snapshot at 03 Pacific Time on 10 September 2017. The red arrows track the movement of the $PM_{2.5}$ plume originating from East Asia. The time elapsed between the first and the last frame is approximately eight days. The movement of the plume illustrates that inter-continental transport from East Asia could contribute to heavily coated rBC-containing particles measured during the first campaign. Concentration colorbar gradient ranges from red to blue, where red represents high concentrations and vice versa.

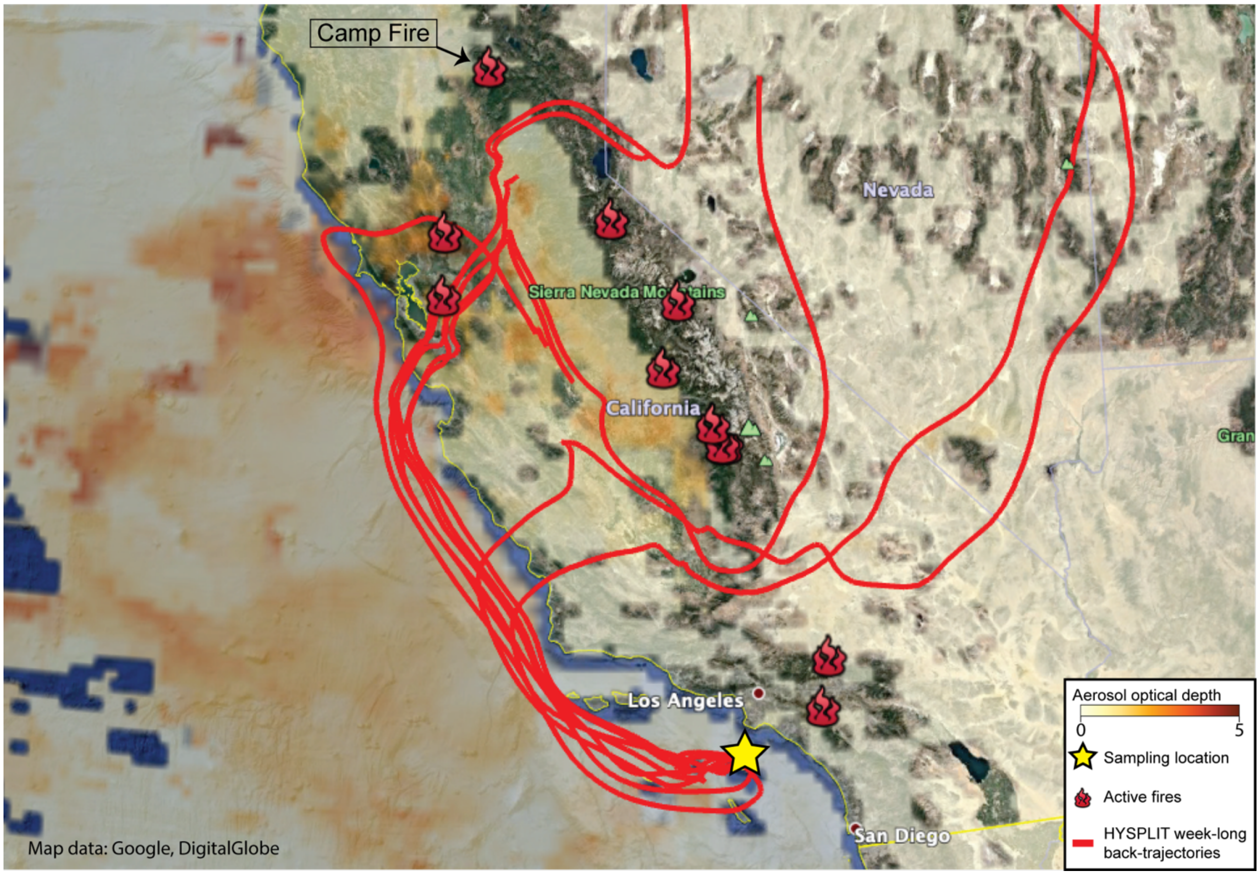

Figure S7. Week-long back-trajectories starting every six hours for the period of elevated f_{BC} between November 16-18, 2018 shown on top of an eight-day averaged AOD layer (9 to 16 November 2018) from MODIS. The AOD scale is shown in the colorbar at the bottom-right corner. The fire symbols represent active fires in Northern and Central California during the time of measurements. The northern-most fire on the map represents the Camp Fire, which encompassed a burn area of more than 600 km^2. Map data © Google Earth.

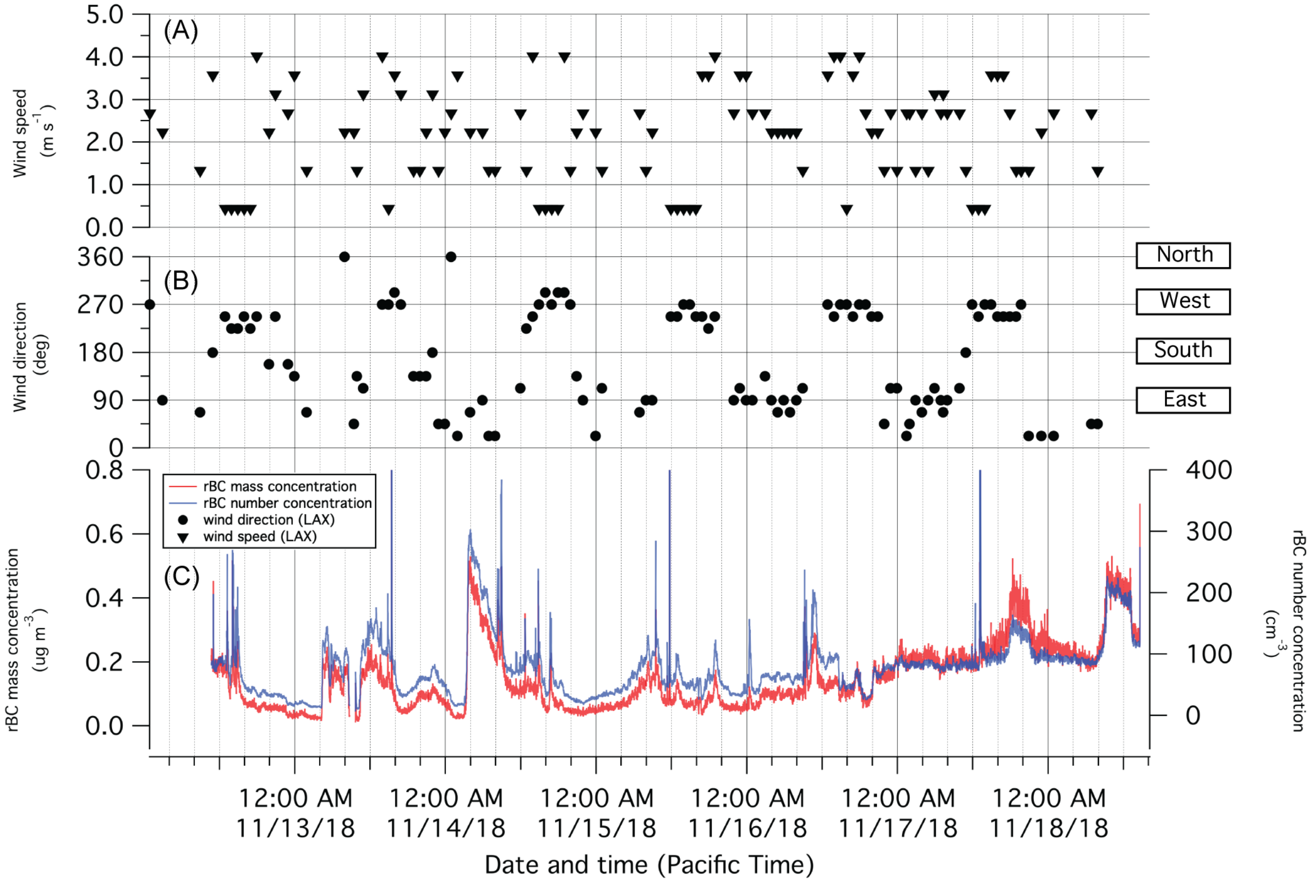

Figure S8. Meteorological variables and rBC concentrations during the third campaign (November 2018). Panel (a) shows wind speed and (b) shows wind direction measured by a NOAA weather station located at Los Angeles International Airport (LAX). Panel (c) shows rBC mass and number concentrations.

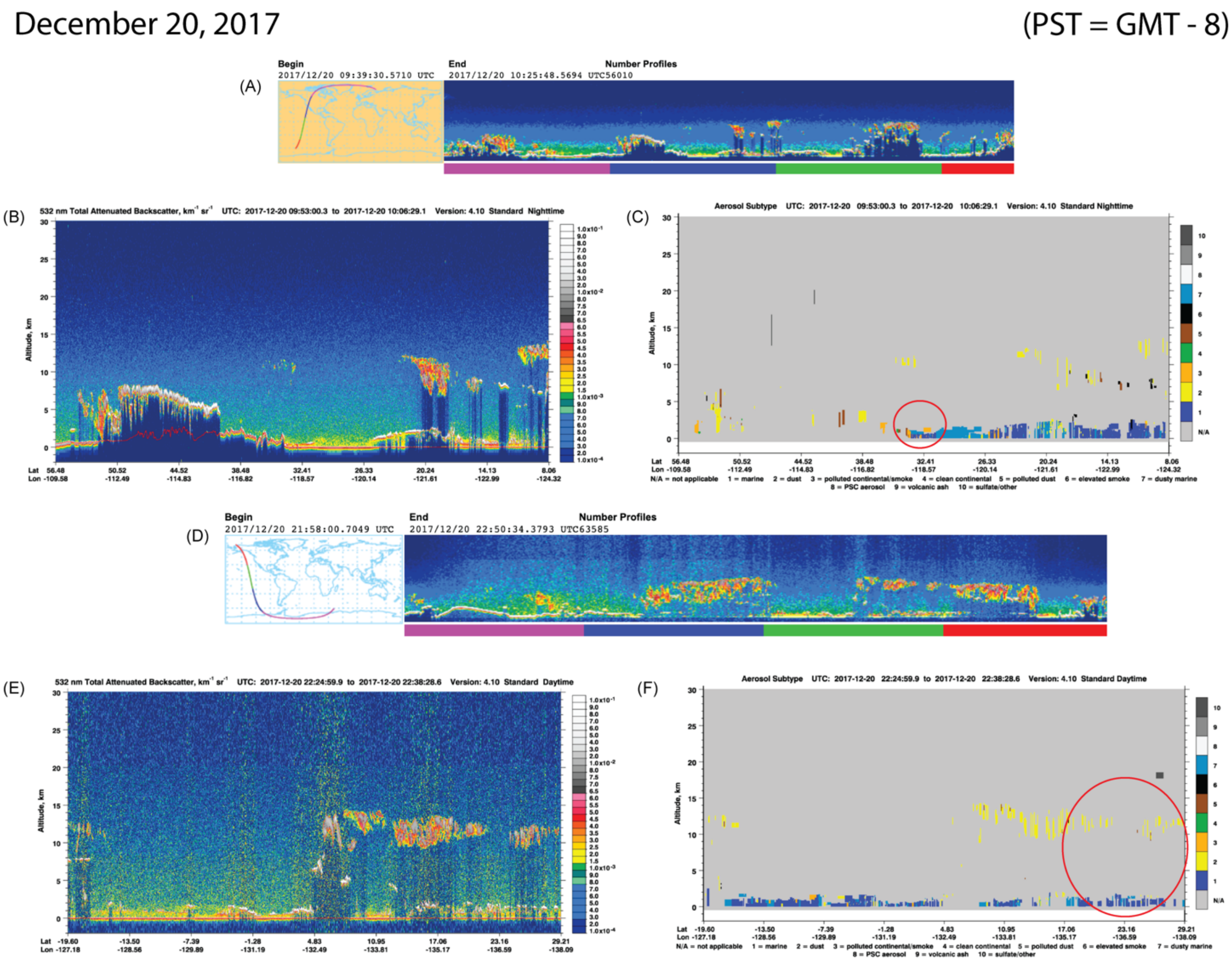

Figure S9. Images collected by NASA's CALIPSO lidar on 20 December 2017. Panel (a) shows the lidar image for the nighttime path, shown in the map on the left. The path is segmented into four parts, separated by different colors. Panel (b) shows the lidar image for the segment of the path that is closest to the Southern California region. Panel (b) shows the aerosol subtypes identified by the CALIPSO automated classification algorithm. Orange, brown, and black areas signify biomass burning aerosols. The same information is shown in panels (d), (e), and (f) for the daytime path, for the same day.

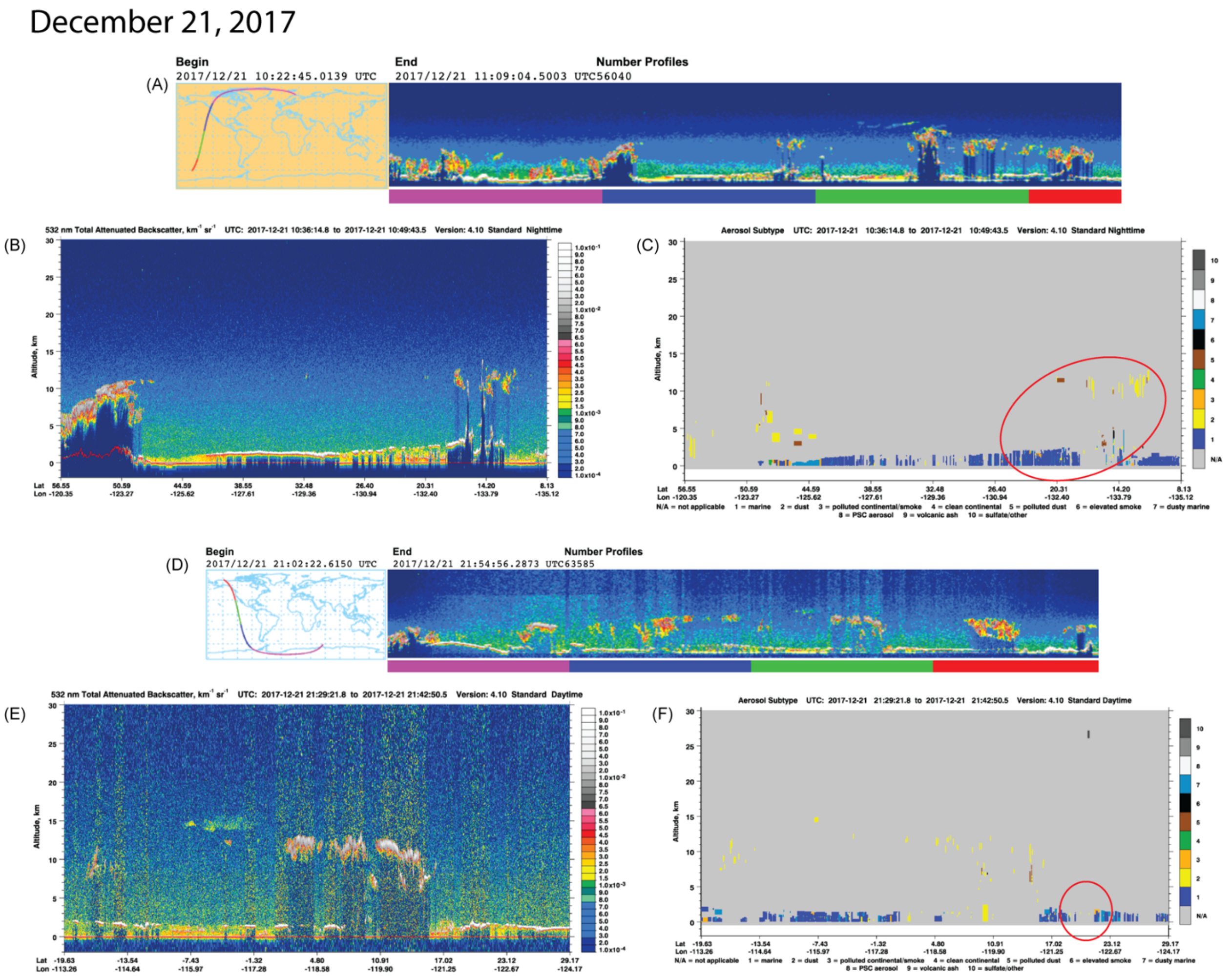

Figure S10. Images collected by NASA's CALIPSO lidar on 21 December 2017. Panel (a) shows the lidar image for the nighttime path, shown in the map on the left. The path is segmented into four parts, separated by different colors. Panel (b) shows the lidar image for the segment of the path that is closest to the Southern California region. Panel (b) shows the aerosol subtypes identified by the CALIPSO automated classification algorithm. Orange, brown, and black areas signify biomass burning aerosols. The same information is shown in panels (d), (e), and (f) for the daytime path, for the same day.

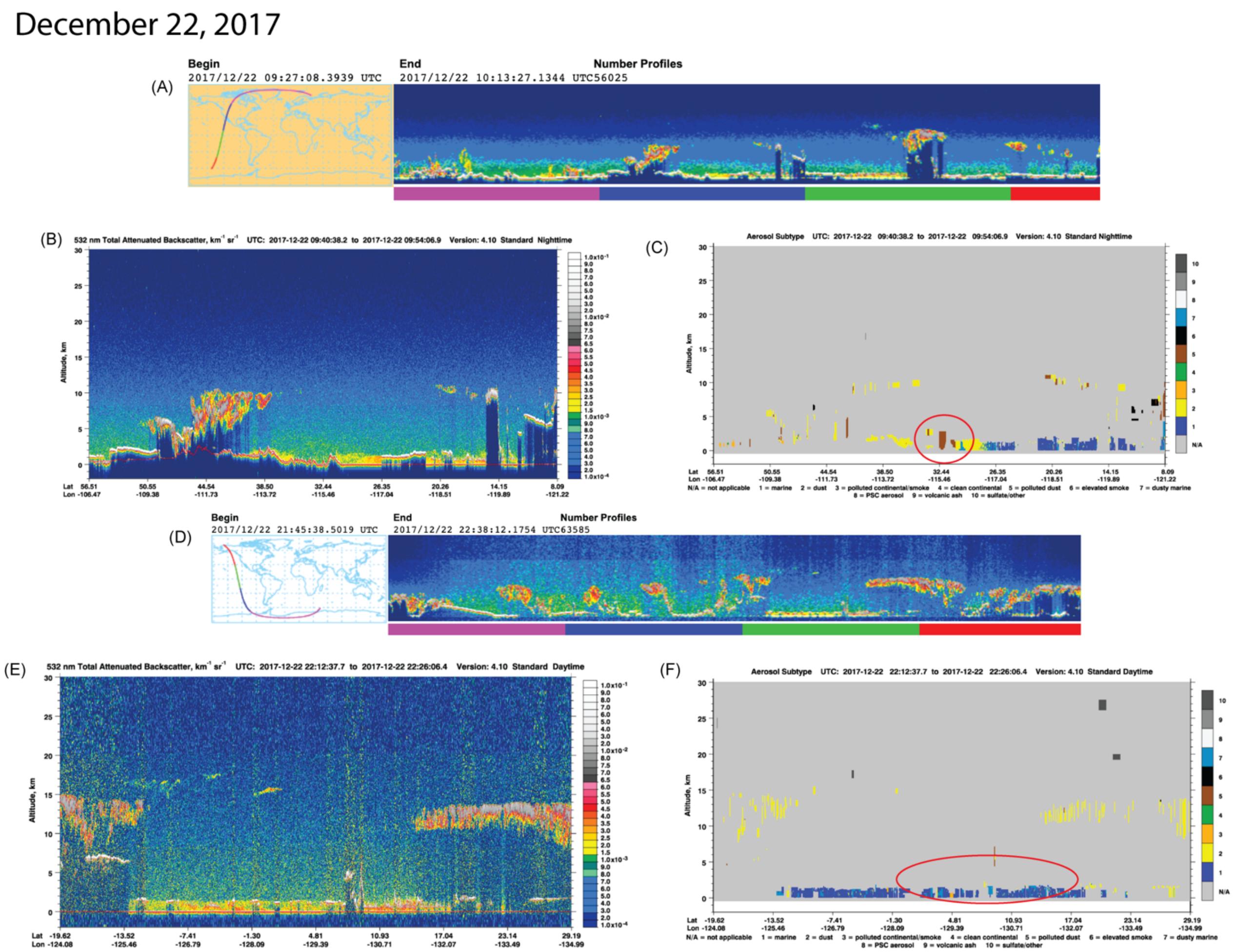

Figure S11. Images collected by NASA's CALIPSO lidar on 22 December 2017. Panel (a) shows the lidar image for the nighttime path, shown in the map on the left. The path is segmented into four parts, separated by different colors. Panel (b) shows the lidar image for the segment of the path that is closest to the Southern California region. Panel (b) shows the aerosol subtypes identified by the CALIPSO automated classification algorithm. Orange, brown, and black areas signify biomass burning aerosols. The same information is shown in panels (d), (e), and (f) for the daytime path, for the same day.

November 12, 2018

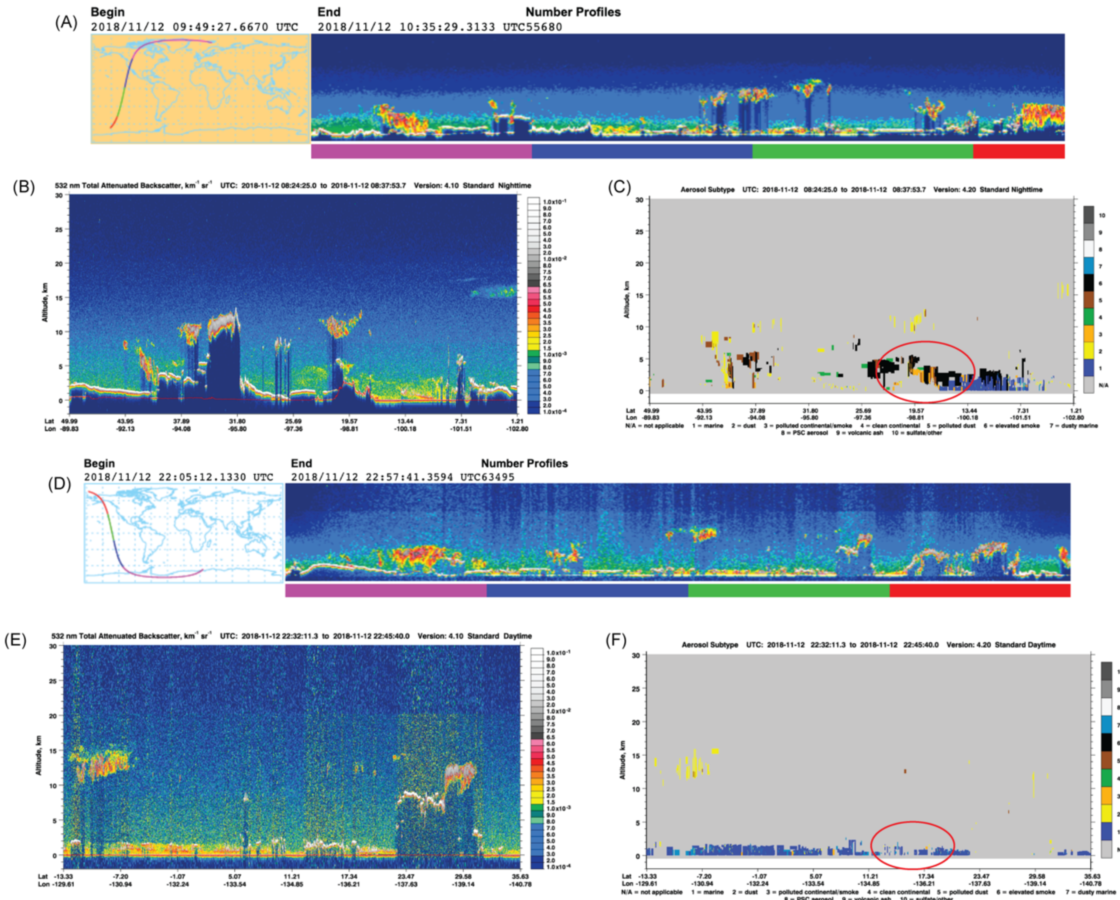

Figure S12. Images collected by NASA's CALIPSO lidar on 12 November 2017. Panel (a) shows the lidar image for the nighttime path, shown in the map on the left. The path is segmented into four parts, separated by different colors. Panel (b) shows the lidar image for the segment of the path that is closest to the Southern California region. Panel (b) shows the aerosol subtypes identified by the CALIPSO automated classification algorithm. Orange, brown, and black areas signify biomass burning aerosols. The same information is shown in panels (d), (e), and (f) for the daytime path, for the same day.

November 13, 2018

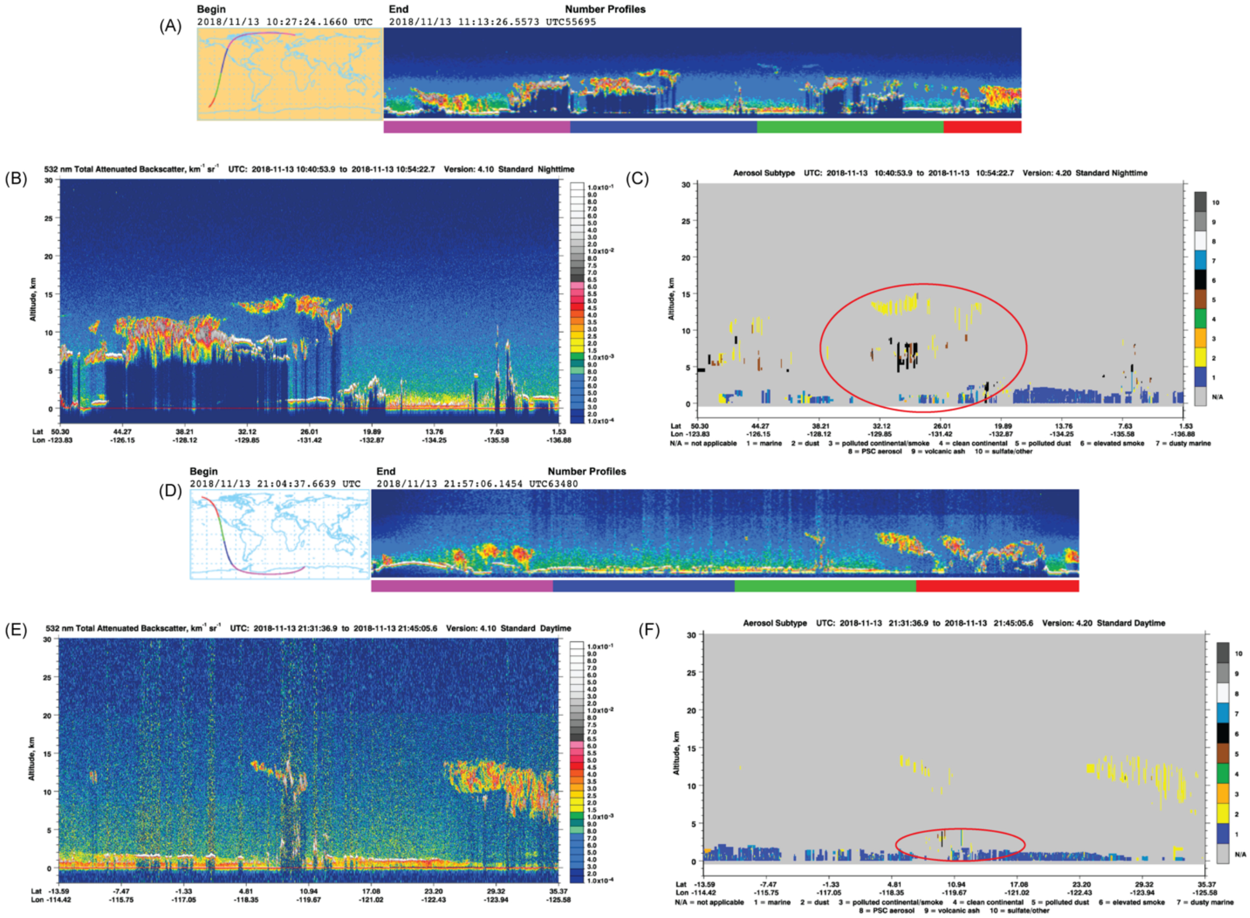

Figure S13. Images collected by NASA's CALIPSO lidar on 13 November 2017. Panel (a) shows the lidar image for the nighttime path, shown in the map on the left. The path is segmented into four parts, separated by different colors. Panel (b) shows the lidar image for the segment of the path that is closest to the Southern California region. Panel (b) shows the aerosol subtypes identified by the CALIPSO automated classification algorithm. Orange, brown, and black areas signify biomass burning aerosols. The same information is shown in panels (d), (e), and (f) for the daytime path, for the same day.

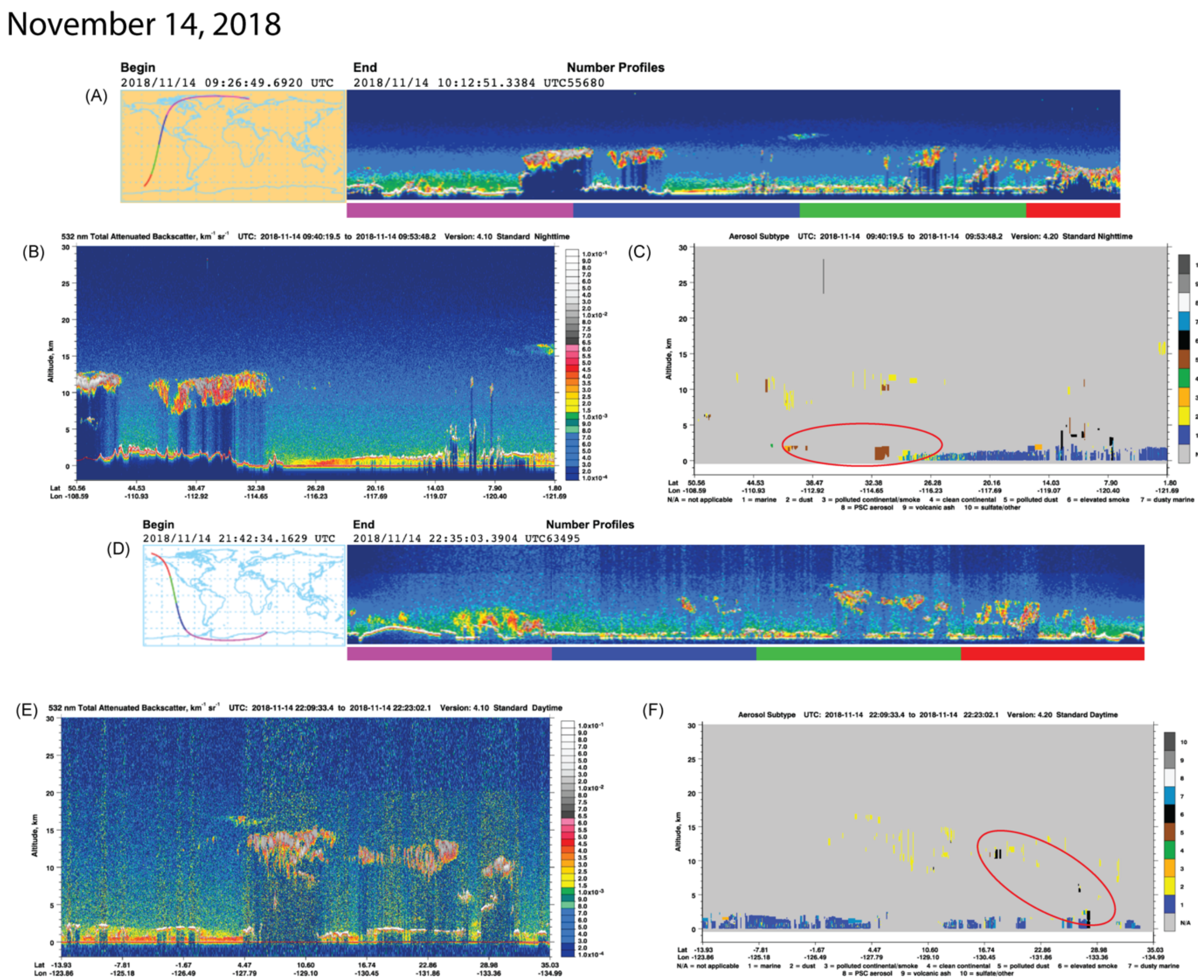

Figure S14. Images collected by NASA's CALIPSO lidar on 14 November 2017. Panel (a) shows the lidar image for the nighttime path, shown in the map on the left. The path is segmented into four parts, separated by different colors. Panel (b) shows the lidar image for the segment of the path that is closest to the Southern California region. Panel (b) shows the aerosol subtypes identified by the CALIPSO automated classification algorithm. Orange, brown, and black areas signify biomass burning aerosols. The same information is shown in panels (d), (e), and (f) for the daytime path, for the same day.

November 15, 2018

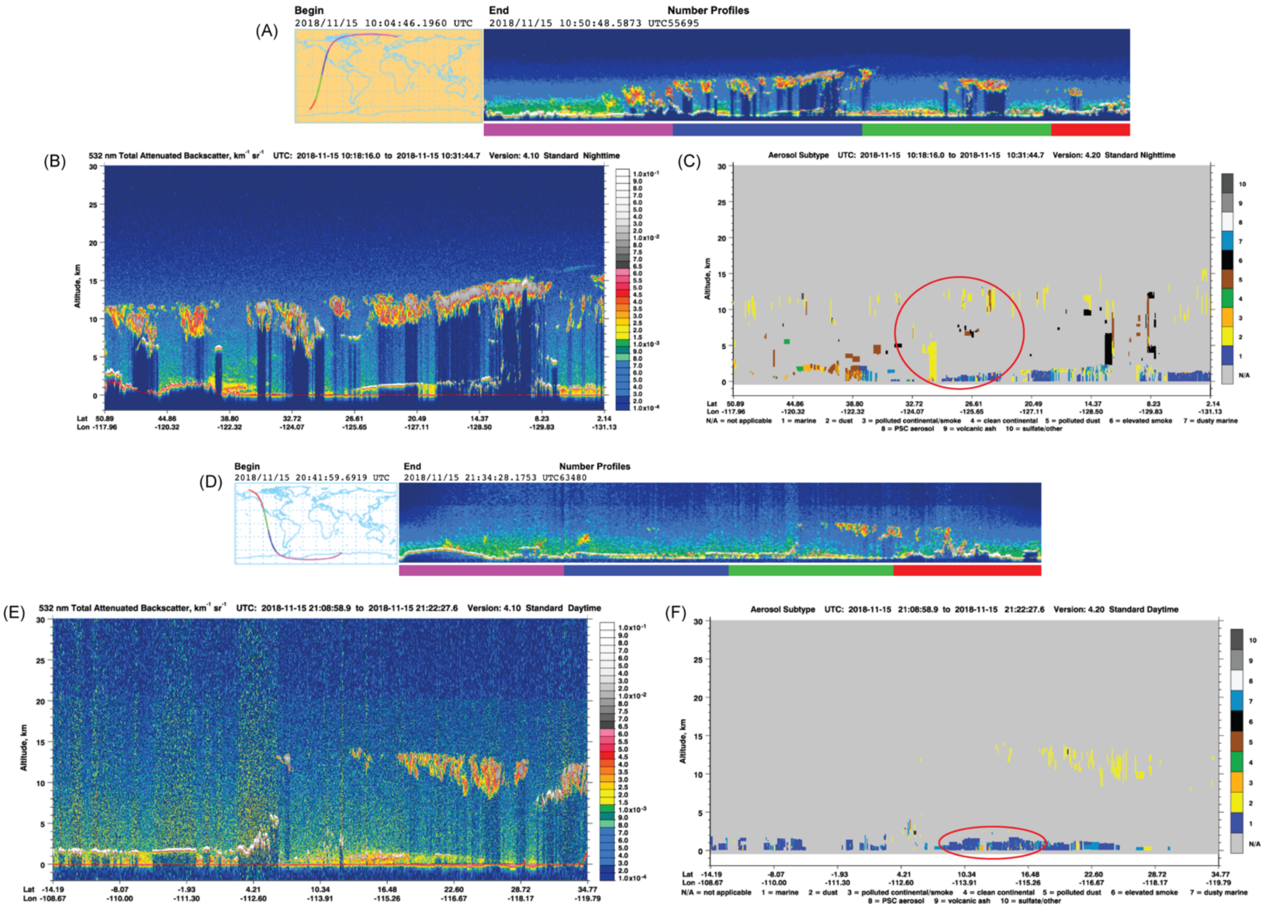

Figure S15. Images collected by NASA's CALIPSO lidar on 15 November 2017. Panel (a) shows the lidar image for the nighttime path, shown in the map on the left. The path is segmented into four parts, separated by different colors. Panel (b) shows the lidar image for the segment of the path that is closest to the Southern California region. Panel (b) shows the aerosol subtypes identified by the CALIPSO automated classification algorithm. Orange, brown, and black areas signify biomass burning aerosols. The same information is shown in panels (d), (e), and (f) for the daytime path, for the same day.

November 16, 2018

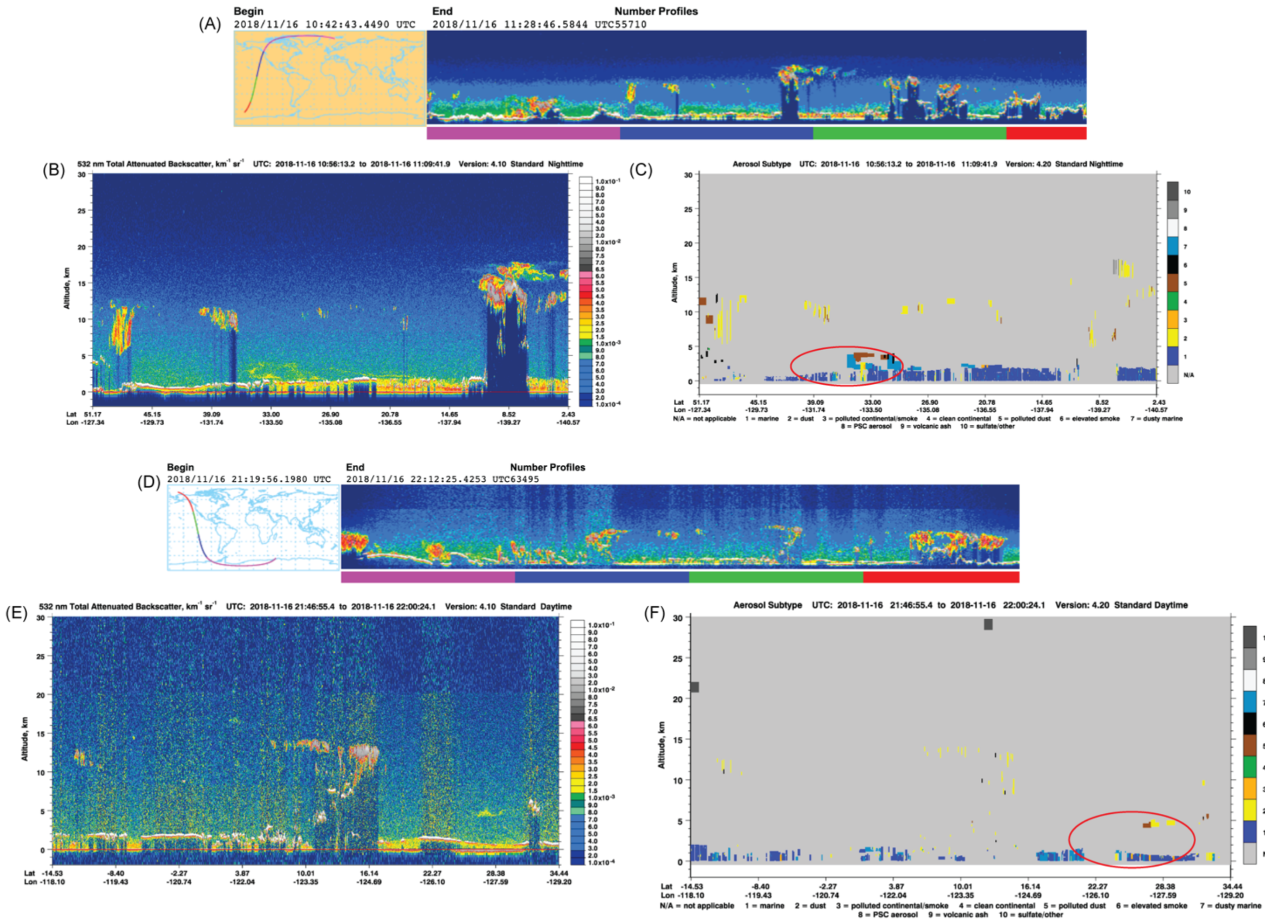

Figure S16. Images collected by NASA's CALIPSO lidar on 16 November 2017. Panel (a) shows the lidar image for the nighttime path, shown in the map on the left. The path is segmented into four parts, separated by different colors. Panel (b) shows the lidar image for the segment of the path that is closest to the Southern California region. Panel (b) shows the aerosol subtypes identified by the CALIPSO automated classification algorithm. Orange, brown, and black areas signify biomass burning aerosols. The same information is shown in panels (d), (e), and (f) for the daytime path, for the same day.

November 17, 2018

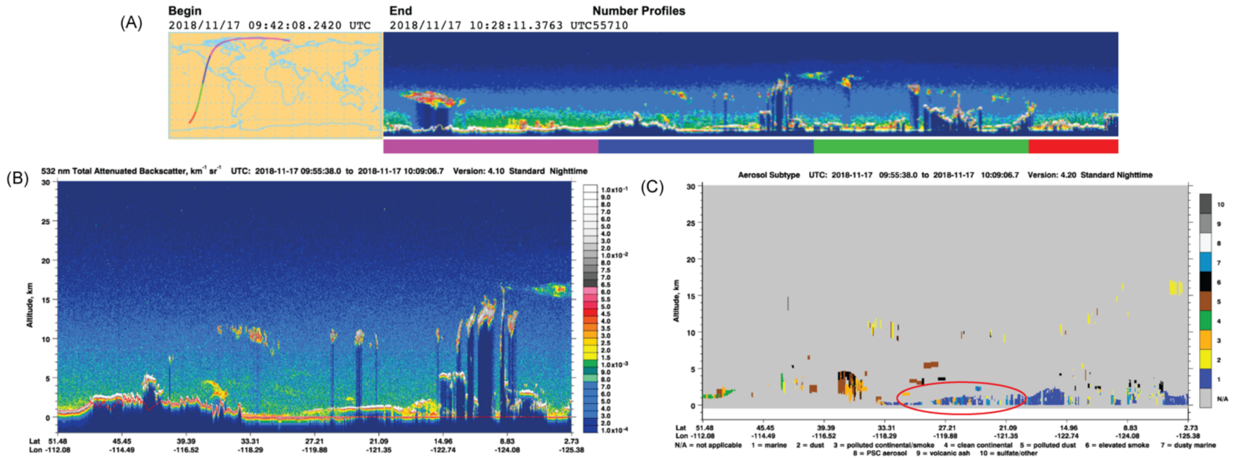

Figure S17. Images collected by NASA's CALIPSO lidar on 17 December 2017. Panel (a) shows the lidar image for the nighttime path, shown in the map on the left. The path is segmented into four parts, separated by different colors. Panel (b) shows the lidar image for the segment of the path that is closest to the Southern California region. Panel (b) shows the aerosol subtypes identified by the CALIPSO automated classification algorithm. Orange, brown, and black areas signify biomass burning aerosols. The image for the daytime transect was not available on this day.

November 18, 2018

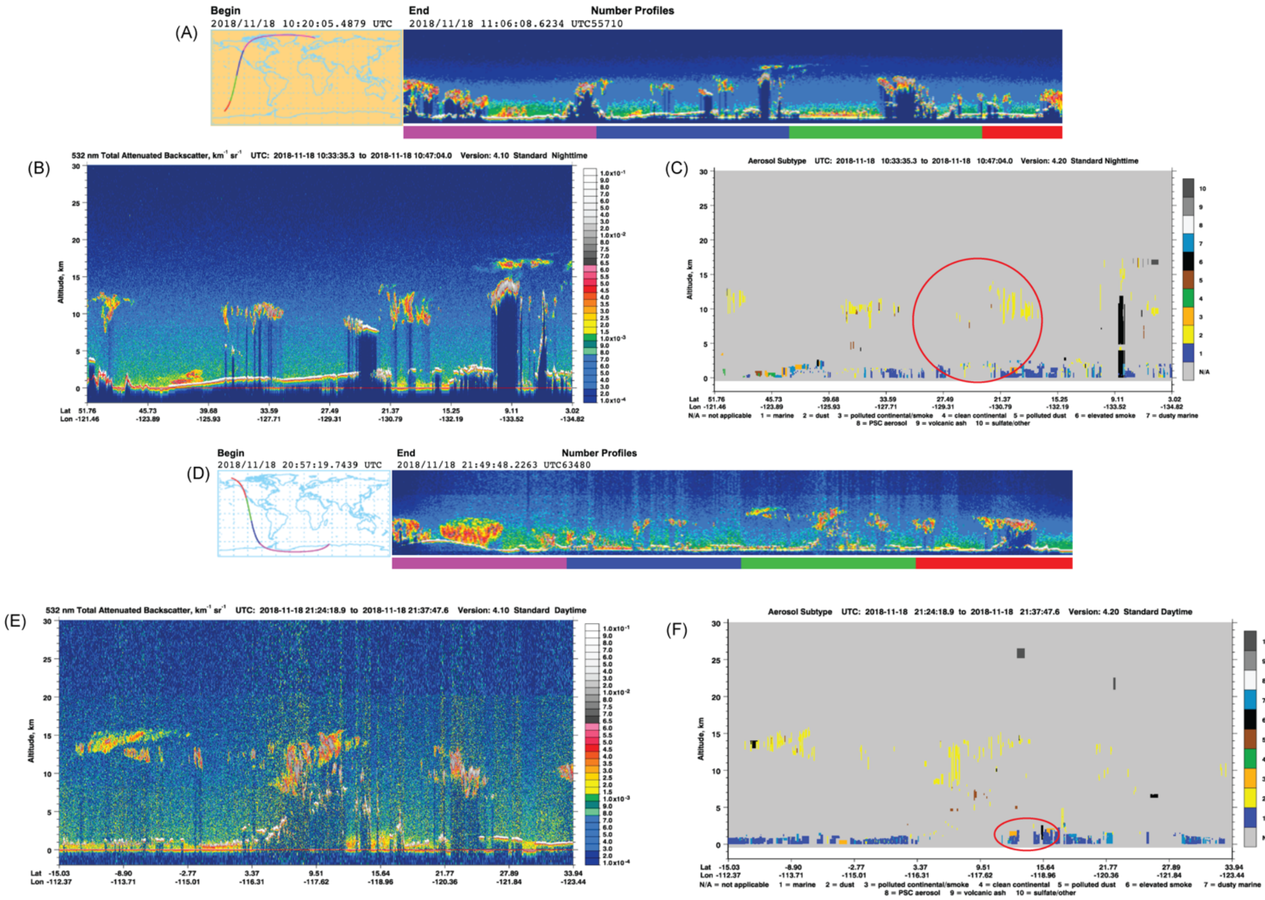

Figure S18. Images collected by NASA's CALIPSO lidar on 18 November 2017. Panel (a) shows the lidar image for the nighttime path, shown in the map on the left. The path is segmented into four parts, separated by different colors. Panel (b) shows the lidar image for the segment of the path that is closest to the Southern California region. Panel (b) shows the aerosol subtypes identified by the CALIPSO automated classification algorithm. Orange, brown, and black areas signify biomass burning aerosols. The same information is shown in panels (d), (e), and (f) for the daytime path, for the same day.

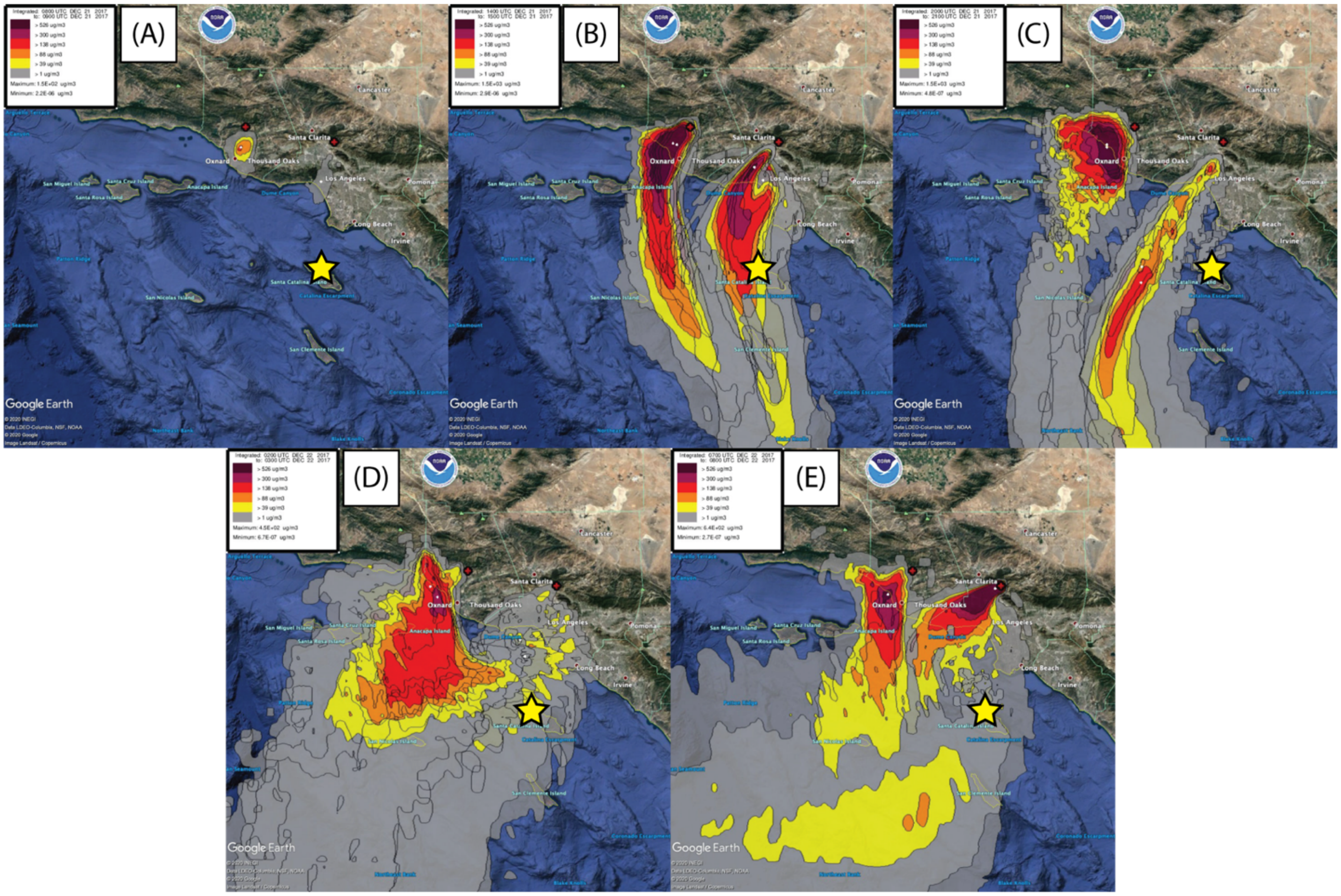

Figure S19. HYSPLIT dispersion model simulating a prescribed burn that encompasses the burn area of the Thomas Fire and Creek Fire. Panel (a) shows the simulation starting on 00:00 Pacific Time on December 21, 2017. Panel (b), (c), (d), and (e) shows concentration isopleths at 06:00, 12:00, 18:00, and 24:00 Pacific Time, respectively. Map data © Google Earth.

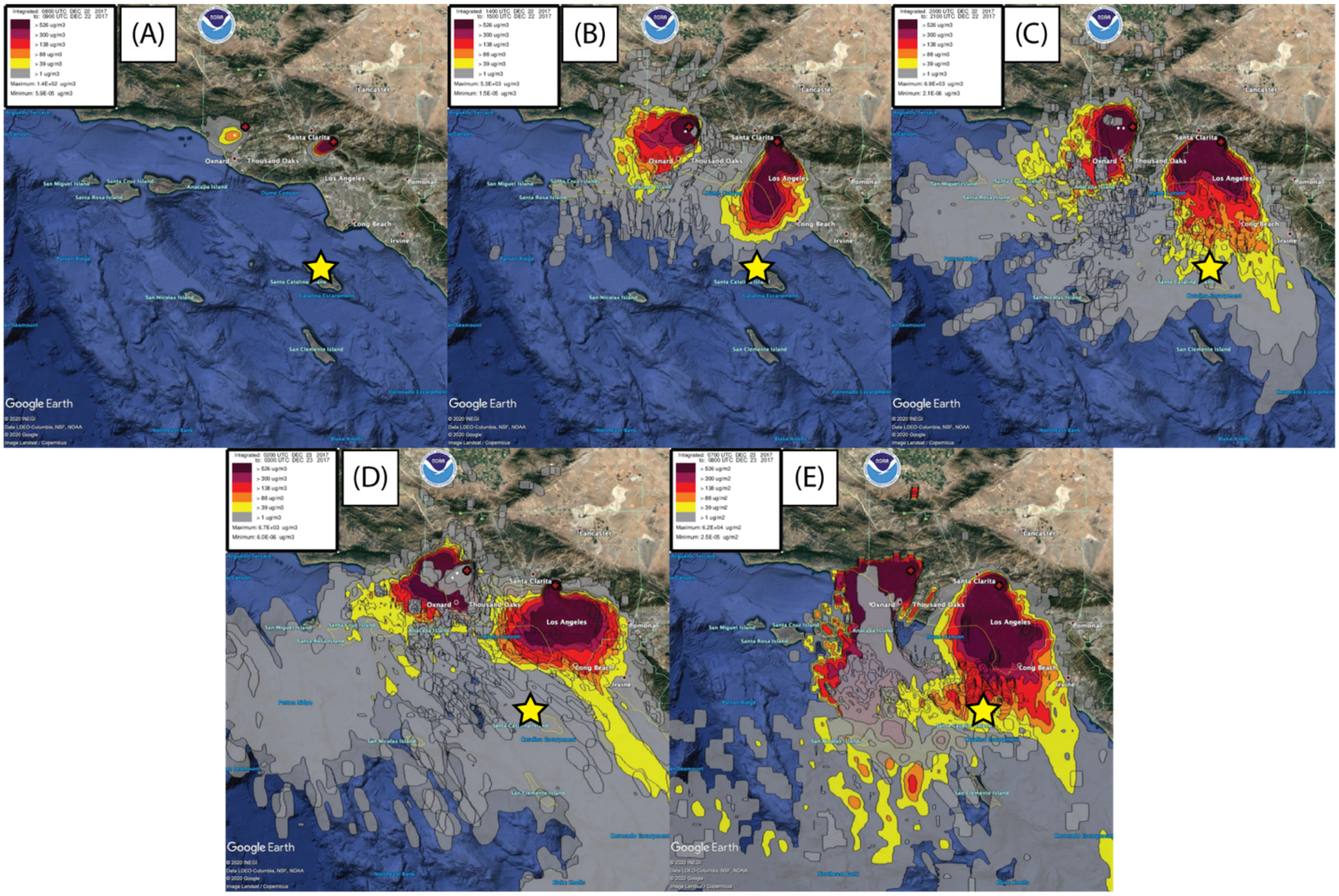

Figure S20. HYSPLIT dispersion model simulating a prescribed burn that encompasses the burn area of the Thomas Fire and Creek Fire. Panel (a) shows the simulation starting on 00:00 Pacific Time on December 22, 2017. Panel (b), (c), (d), and (e) shows concentration isopleths at 06:00, 12:00, 18:00, and 24:00 Pacific Time, respectively. Map data © Google Earth.

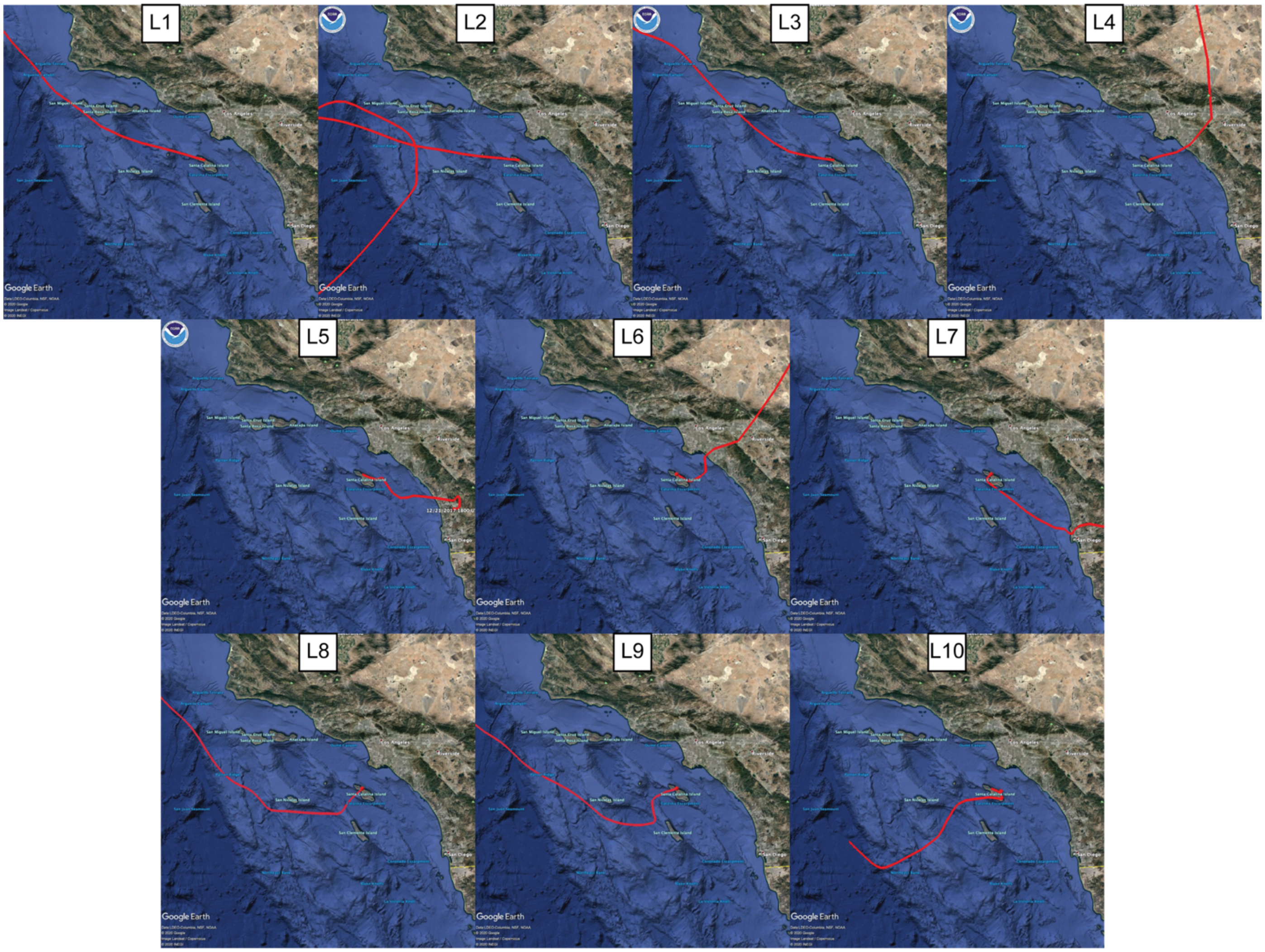

Figure S21. HYSPLIT back-trajectories for LEO periods L1 through L10. See section 2.3 of manuscript for details regarding HYSPLIT. Map data © Google Earth.

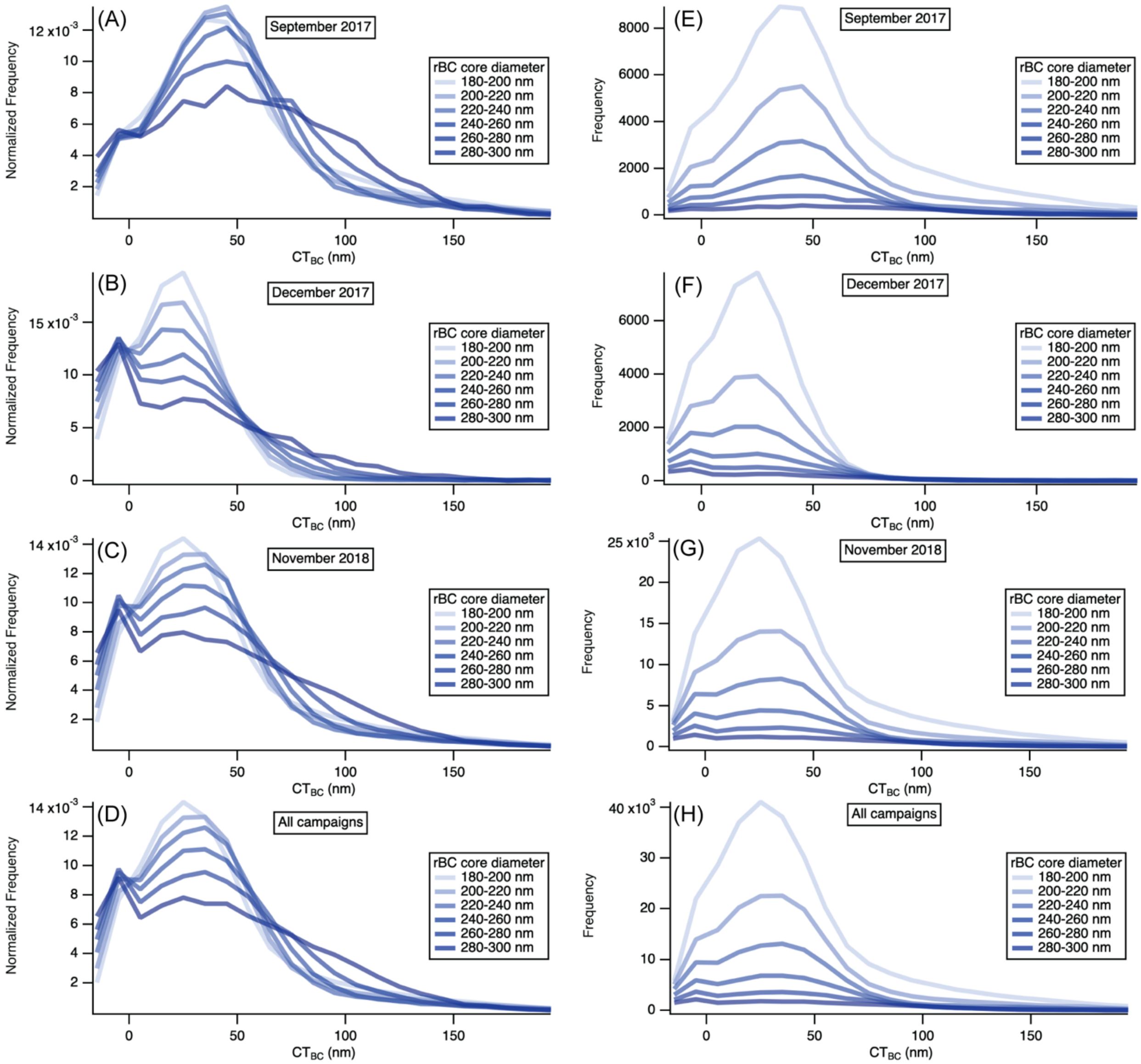

Figure S22. Distributions of BC coating thickness (CT_{BC}) aggregated by campaign and varying rBC core diameter ranges used in the LEO analysis. Panels (a) through (d) in the left column show the normalized frequency distributions, while panels (e) through (h) in the right column show the absolute frequency distributions. Within each panel, each line represents a distribution for a particular rBC core diameter range, with darker lines representing larger diameter ranges and vice versa.

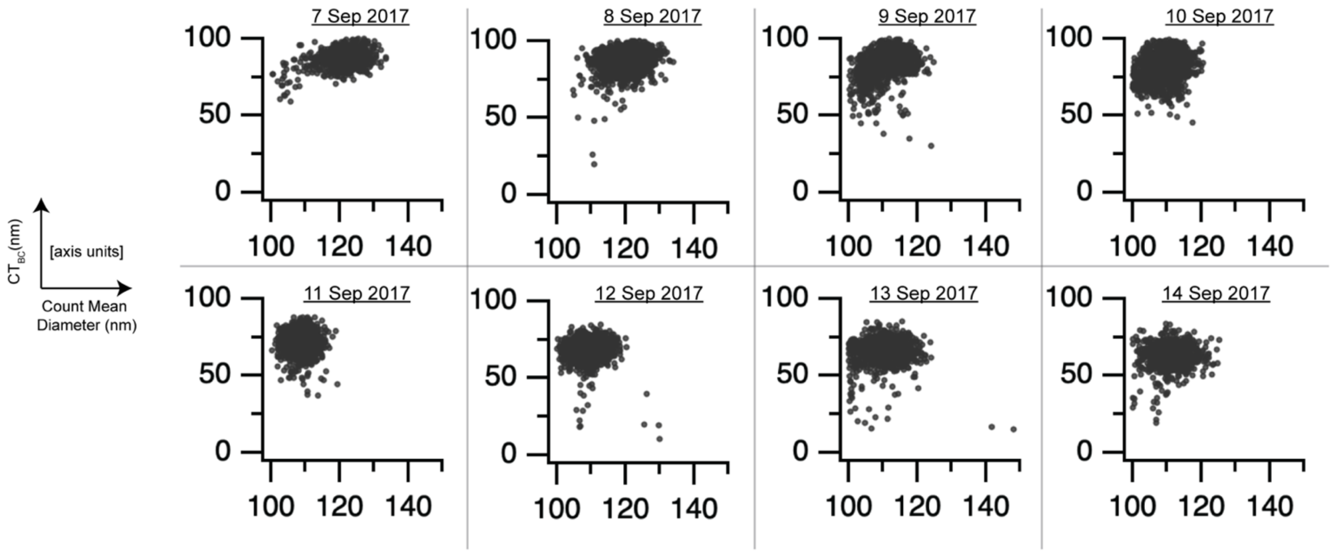

Figure S23. Scatter plots for each day of the first campaign (September 2017), as a function of BC coating thickness (CT_{BC}) and rBC count mean diameter. Each point represents a one-minute mean value.

References

Soleimanian, E., Mousavi, A., Taghvaee, S., Shafer, M. M., and Sioutas, C.: Impact of secondary and primary particulate matter (PM) sources on the enhanced light absorption by brown carbon (BrC) particles in central Los Angeles, Sci. Total Environ., 705, 135902, https://doi.org/10.1016/j.scitotenv.2019.135902, 2020.